CHEMIJA
2025. Vol. 36. No. 3. P. 197–205

ISSN 0235-7216 eISSN 2424-4538
DOI: https://doi.org/10.6001/chemija.2025.36.3.8

The use of physics-informed neural networks (PINNs) to map the Zn^{2+} nanoparticles diffusion in Swiss chard: an AI simplified modelling approach

Mohamed Abdelkader[1],

Simona Tučkutė[2*],

Rasa Pauliukaitė[1]

[1] *Department of Nanoengineering, Center for Physical Sciences and Technology (FTMC), 231 Savanorių Street, 02300 Vilnius, Lithuania*

[2] *Lithuanian Energy Institute, 3 Breslaujos Street, 44403 Kaunas, Lithuania*

Electrochemical processes are central to energy storage, catalysis, corrosion and sensing, yet understanding and optimising these systems remains challenging. Physics-informed neural networks (PINNs) offer a promising approach by integrating physical laws into machine learning models for improved interpretability and accuracy. In this work, we develop a PINN to simulate the diffusion and electric-field-driven transport of Zn^{2+} ions released from ZnO nanoparticles in the beetroot – Swiss chard – leaf tissue. The model embeds the Poisson's equation for electric potential and the Nernst–Planck equation for ion flux into the network's loss function, enabling it to learn physically consistent potential and concentration fields with minimal data. The PINN predictions reveal that Zn^{2+} ions accumulate near leaf edges, a phenomenon also observed experimentally. Using the trained model, we evaluate microelectrode sensor array designs and find that a hexagonal electrode layout would capture the edge-concentrated Zn^{2+} distribution more effectively than a uniform grid. This case study demonstrates how AI modelling informed by physics can accurately replicate experimental trends and guide the design of better electrochemical sensors. The results highlight the broader potential of PINNs to advance electrochemical research by combining data-driven learning with established physical electrochemical principles.

Keywords: physics-informed neural networks, electrochemistry, diffusion modelling, microelectrode array, Swiss chard leaf

INTRODUCTION

Electrochemistry is pivotal in energy storage, catalysis, corrosion prevention, sensing, and chemical synthesis. Electrochemical sensing is one of the application areas of electrochemistry, and it is experiencing a renaissance due to the need for a wide variety of minimised sensors for the Internet of Things (IoT) approach [1].

Recent advances in artificial intelligence (AI) and machine learning (ML) have begun to revolutionise these areas by accelerating discovery and optimising complex systems [2, 3]. AI increasingly shapes how researchers tackle challenging scientific questions, opening doors we never knew existed. While some fear machines replacing human intuition, others see AI as an advanced tool that complements our natural curiosity. The application of AI and ML in electrochemistry has expanded rapidly in recent years, encompassing energy storage, corrosion, sensing, catalysis, and more [4]. Physics-informed neural networks (PINNs) are a class of deep learning models that embed governing physical laws (expressed as differential equations) into

* Corresponding author. Email: simona.tuckute@lei.lt

the training process [5]; researchers increasingly view PINNs as a pathway to more explainable machine learning, as embedding prior scientific knowledge leads to 'better accountability, interpretability, and generalization' in predictive models [6]. By incorporating scientific domain knowledge directly into the loss function, PINNs ensure solutions that are consistent with known physics while reducing reliance on large datasets. Since their introduction by Raissi et al., PINNs have gained popularity across many fields of science and engineering; in particular, they have been widely applied to model and analyse complex systems such as lithium-ion batteries and fuel cells [5, 7].

AI/ML techniques are seen as a huge shift in electrochemistry, e.g. battery research, enabling a faster development by handling high-dimensional data beyond human intuition [8, 9]. Data-driven models can predict battery aging and state-of-health, supplementing or even surpassing traditional physics-based models when large datasets are available [8, 10]. Beyond batteries, AI has penetrated electrocatalysis, corrosion science, sensing, and reaction discovery. In electrocatalysis, which drives processes like water splitting and CO_2 reduction, determining optimal catalyst compositions and conditions is a complex, time-intensive task. Recent studies show that ML can greatly accelerate catalyst optimisation, saving significant time and resources [11]. For instance, ML models have been used to screen catalyst shapes or alloy compositions to maximise activity/selectivity, rapidly narrowing design candidates. Likewise, physics-informed ML strategies are being explored in catalysis to incorporate reaction kinetics and thermodynamics into predictive models [12], yielding more interpretable guidance for catalyst development. In corrosion modelling, data-driven approaches help predict material degradation and identify protective measures. ML models have been trained to predict corrosion potential and current for various alloys with a good accuracy [13]. However, a common challenge in corrosion research is the scarcity of large labelled datasets (e.g. electrochemical measurements under diverse conditions). Here, advanced deep learning techniques like generative adversarial networks (GANs) are being used to expand datasets synthetically [14].

Electrochemical sensors and biosensors are another domain benefitting from AI. ML methods – often coupled with chemometrics – are employed to analyse complex voltametric or impedance data, improving sensitivity and multi-analyte detection [15]. Nonlinear patterns in sensor responses that were previously difficult to quantify can be trained by ML, leading to a more accurate calibration and analyte classification [16, 17].

Across all these applications, a key insight is that purely data-driven models, while powerful, often suffer from a limited interpretability and may require infeasibly large datasets for complex electrochemical systems. This has led to a growing interest in PINNs and related approaches that embed physical laws into AI models. PINNs are a class of neural networks trained not only on data but also on physical governing equations as part of the loss function or model architecture.

The newest trends in agricultural sciences are foliar fertilisation. Moreover, sensors are being developed to monitor the concentration of nutrients needed to prevent both overfertilisation and deficiency [18] with Zn-containing nanoparticles (NPs) and expect that leaf biota might digest them and transfer the compounds. Zn, as a microelement for plants, usually comes from soil and can be taken in the form of soluble chelate complex compounds via roots [19]. It is usually present in Earth's core in the form of minerals such as Zn carbonates (smithsonite), Zn silicates (hemimorphite), or Zn sulphides (sphalerite and wurtzite) [20]. Microorganisms of soil biota transform these minerals into soluble complex compounds. Since Zn-containing NPs are commercially available as ZnO, they were tested as a possible candidate, expecting that leaf biota would convert them into Zn^{2+}.

Electrochemical sensors provide a practical and highly sensitive platform for the *in situ* detection of metal ions, including Zn^{2+}, in complex biological matrices. Zn is a critical micronutrient in plants, influencing enzymatic catalysis, gene expression, and cellular structure. Its deficiency leads to stunted growth and reduced yield, while excess becomes phytotoxic. Accordingly, the electroanalytical quantification of Zn^{2+} in plant tissues is vital for understanding nutrient transport, evaluating bioavailability, and informing agronomic interventions [21, 22]. Electrochemical techniques, owing to their portability, low cost, and suitability for miniaturisation, are ideally positioned to address this analytical challenge [23].

In this work, we explore the usage of PINNs in electrochemistry through a case study of electrochemical Zn^{2+} detection in plant tissues. We first summarise the governing equations and the PINN model architecture used to simulate Zn^{2+} ion transport and electric potential in a Swiss chard leaf. The PINN is trained to satisfy Poisson's equation for the electric field and the Nernst–Planck equation for ionic diffusion-migration, embedding these laws into the neural network (NN). Next, we present the results of the PINN simulation, including the predicted potential and concentration fields, and compare them against experimental observations. We also evaluate different designs for a microelectrode sensor array (uniform grid vs hexagonal pattern) informed by the model's predictions. In the discussion, we analyse how PINN's physics-based modelling explains why ZnO nanoparticles accumulate at leaf edges and how the model-guided electrode design can improve detection. This case study thus validates the PINN approach's ability to accurately capture electrochemical phenomena with improved interpretability and reduced data needs. We conclude with perspectives on the broader significance of AI and PINNs in advancing electrochemical research, highlighting the balance of data and physics in next-generation modelling.

EXPERIMENTAL

Governing equations and physical model

The electrochemical detection of Zn^{2+} in a leaf can be described by coupled field equations for the electric potential and ion concentration. We employed the Poisson–Nernst–Planck (PNP) equation, which is commonly used to model ionic transport in an electrochemical system [24].

The PNP model comprises Poisson's equation for the electric potential (φ) and the Nernst–Planck equation for the concentration (c) of Zn^{2+} ions. Under steady-state conditions (time-invariant fields), the Poisson's equation is used:

$$\nabla (\varepsilon \nabla \varphi) = -\rho, \quad (1)$$

where ε is the permittivity of the medium (leaf tissue), and ρ is the volume charge density. This equation relates the spatial variation of the electric potential to the local charge density (by Gauss's law). For simplicity, ε is treated as constant, and ρ is primarily due to Zn^{2+}, linked directly to the ion concentration. Nernst–Planck equation

$$\nabla J = R \quad (2)$$

is used with the ionic flux J given by

$$J = -D\nabla c + \mu c \nabla \varphi, \quad (3)$$

where D is the diffusion coefficient of Zn^{2+}, μ is the ionic mobility, and R is the reaction term for ion generation or consumption. Here, J comprises a diffusive term driving ions from higher to lower concentrations and an electrophoretic term moving ions along the electric field gradients. Under steady-state (achieved several minutes after ZnO nanoparticle application), time derivatives vanish. A characteristic diffusion timescale supports this assumption: with leaf thickness L ~0.5 mm and diffusion coefficient D ~7×10^{-10} m^2/s, the diffusion time is

$$t_{diff} \approx L^2/D \approx 360\ s\ (\sim 6\ \text{minutes}). \quad (4)$$

Charge density ρ is linked to Zn^{2+} concentration, assuming dominant charge carriers: $\rho \approx zFc$, where $z = 2$ and F is the Faraday's constant. An experimental ZnO concentration of 0.19 mg/L corresponds to $\rho \approx 2.91 \times 10^{-6}$ mol/m^3, used as a representative. Relative permittivity $\varepsilon_r \approx 50$ translates to absolute permittivity $\varepsilon \approx 50 \times 8.85 \times 10^{-12}$ F/m. $D = 7 \times 10^{-10}$ m^2/s and $\mu = 1.7 \times 10^{-8}$ $m^2/(V \cdot s)$ were used, based on typical Zn^{2+} ion properties and the Nernst–Einstein relation at room temperature (298 K).

For simplicity, the reaction term was set constant at $R = 1.0$ (normalised units), representing the uniform Zn^{2+} generation from nanoparticles. The PINN implicitly handles boundary conditions, assuming no-flux boundaries (preventing rapid loss at leaf edges), and a reference potential φ defined relative to zero at the boundary. Without explicit Dirichlet conditions, PINNs naturally learn a consistent reference potential due to the coupling between φ and c. These realistic parameters ensure that PINN operates in a physically accurate regime, effectively capturing the steady-state distribution of Zn^{2+} within the leaf structure. The PINN approach implicitly handles

the boundary conditions (described below). We assume no-flux boundaries for the concentration (leaf edges do not rapidly lose Zn^{2+}, or any loss is balanced by intake from adjacent tissue) and a reference potential such that φ is defined relative to zero at the boundary. In practice, the PINN can learn an effective potential profile without explicitly enforcing Dirichlet boundary conditions as long as a consistent reference emerges (only differences in φ matter for the physics). We do note that without a fixed reference, Poisson's equation has gauge freedom (adding a constant to φ); however, the coupling to concentration in Nernst–Planck typically pins the potential when a steady state with sources is reached.

PINN architecture and training

We implemented a single neural network PINN [25] that outputs both the electric potential $\phi(x, y)$ and the Zn^{2+} concentration $c(x, y)$ as functions of position in the 2D leaf cross-section. The input features to the network are the spatial coordinates (x, y) which we normalised to the unit square $[0.1] \times [0.1]$ representing the region of interest in the leaf. The network architecture consists of several fully connected hidden layers with nonlinear activation functions, and two outputs corresponding to ϕ and c. In our implementation, we used 3 hidden layers with 64 neurons each and tanh activations (a common choice in PINNs for smooth function approximation) for the hidden layers. The output layer is linear (no activation) to produce the real-valued potential and concentration. This relatively compact architecture was sufficient to approximate the smooth spatial profiles of ϕ and c in the leaf:

$$\mathcal{L} = \frac{1}{N}\sum_{i=1}^{N}[\nabla\cdot(\varepsilon\nabla\phi(x_i,y_i)) + \rho(x_i,y_i)]^2 + \frac{1}{N}\sum_{i=1}^{N}[\nabla\cdot(-D\nabla c(x_i,y_i)) + \mu c(x_i,y_i)\nabla\phi(x_i,y_i)) - R]^2, \quad (5)$$

where the summations are over N collocation points (x_i, y_i) randomly distributed in the domain. In essence, the network adjusts its weights so that it outputs ϕ and c fields that make these PDE residuals as small as possible at all sampled points. By training to minimise this physics-based loss, the PINN is to produce solutions that satisfy Gauss's law and ion transport conservation everywhere, rather than simply interpolating data. We included a small additional penalty in the loss for known boundary conditions or symmetry as needed (for example, enforcing $\phi = 0$ at the boundary in an early stage as a reference).

Training was performed using a gradient-based optimizer (Adam) to iteratively minimise the loss. We initialised N = 100 collocation points uniformly across the 2D leaf domain for computing the residuals. The PINN was trained for up to 10,000 epochs with an initial learning rate of 10^{-3}. We employed an early stopping criterion: if the loss fell below a threshold (10^{-5} in normalised units) or stopped improving significantly, training was halted early to prevent overfitting or unnecessary computation. From the computations, the model converged well before the maximum epochs. During each training epoch, we used automatic differentiation to compute the necessary spatial derivatives in the residual terms, as shown in Eq. (5) with respect to (x, y), as well as the gradients of the loss with respect to the network weights. This was implemented using TensorFlow's built-in automatic differentiation (gradient tape) capability in Python, which allowed obtaining exact derivatives of the network outputs with respect to inputs for the PDE residuals. These were then combined as per the equations to evaluate the loss, and the weight gradients were obtained via backpropagation.

Despite the complexity of the coupled equations, the PINN training was stable and converged to a low-loss solution. The final training loss achieved was on the order of 10^{-6}, indicating that the network's predictions satisfy the Poisson and Nernst–Planck equations to a high accuracy (with very small residuals) throughout the domain. After training, we validated the PINN by evaluating $\phi(x, y)$ and $c(x, y)$ on a fine grid of points covering the leaf area, effectively obtaining continuous predictions for the potential field and concentration field. The PINN solution is mesh-free, but for visualisation purposes, we sampled it on a 100×100 grid to generate smooth contour plots of ϕ and c. The results of this PINN simulation are presented in the next section. Additionally, the simulations were conducted in two modes: (1) using nondimensional (arbitrary) units for the different parameters and constants during initial development to ensure that the PINN could find a consistent solution, and

(2) with the realistic physical constants and units given above to tie the predictions to expected actual data. The qualitative behaviour of the solution was similar in both cases, but using real units allowed the direct comparison of the predicted concentrations and potentials with experimental measurements (in absolute terms).

Scanning electron microscopy

Scanning electron microscopy (SEM) was used to examine the microstructural features of the Swiss chard (*Beta vulgaris* subsp. *cicla*) leaf surface. SEM characterisation was carried out using a Hitachi S-3400N scanning electron microscope. To preserve the intrinsic morphology, no conductive coating was applied to the specimens prior to imaging. This non-coated approach was deliberately employed to avoid potential topographical alterations or artifacts typically introduced by sputter-coated conductive layers, thereby ensuring that the acquired images faithfully represent the native leaf surface. Imaging was performed at a low accelerating voltage of 3 keV, which enhances surface-sensitive resolution while minimising electron beam–induced charging and structural damage in non-conductive biological samples. The resulting micrographs provided high-fidelity visualisation of the epidermal architecture, including stomatal distribution and cuticular features, which were further correlated with the modelled Zn^{2+} transport phenomena described in this study.

RESULTS AND DISCUSSION

The transport of Zn^{2+} ions in a Swiss chard (*Beta vulgaris* subsp. *cicla*) leaf was simulated using a PINN under steady-state conditions. To enable tractable computation, the leaf was approximated as a symmetric laminar domain with a continuous permittivity and diffusivity – reasonable assumptions when vascular architecture is diffuse or secondary at the scale of interest [26], as shown in Fig. 1. These simplifications permit the application of Poisson and Nernst–Planck equations to describe the coupling of electrostatic potential and ion migration within the leaf mesophyll, when treating the mesophyll as a porous electrolyte domain with ion-selective dynamics [27].

As shown in Fig. 2, the PINN predicts a smooth electric potential field within the leaf, highest in the interior region and lowest at the boundaries. Quantitatively, the potential ϕ is on the order of 10^{-3} in the centre and approaches zero at the outer leaf edges. This results in a roughly shaped potential profile, with the leaf centre at a slightly positive potential relative to the edges. Physically, this behaviour makes sense: the accumulation of positive charge (Zn^{2+} and any other ions) in the tissue interior leads to a build-up of electric potential that contains the charge. Poisson's equation reflects the local charge density, so regions with more Zn^{2+} (the centre of the leaf, initially) have a higher ϕ. The potential decreases smoothly toward the edges, where the charge density drops off, and we observe

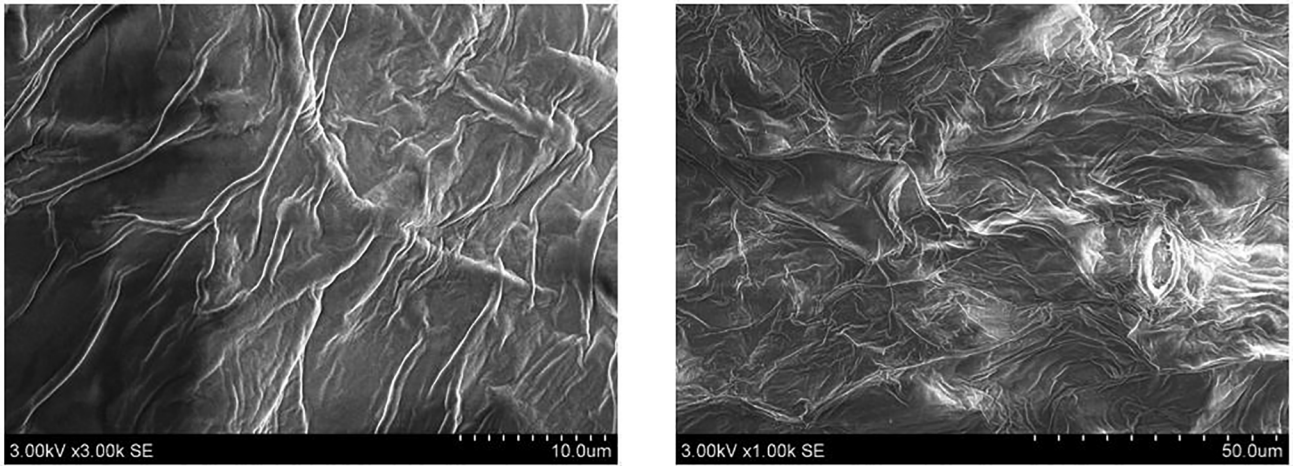

Fig. 1. SEM images of the Swiss chard leaf surface: (a) higher magnification view (scale bar: 10 μm) revealing the wrinkled surface topography and fibrous structures; (b) lower magnification view (scale bar: 50 μm) showing a broader surface morphology including stomata

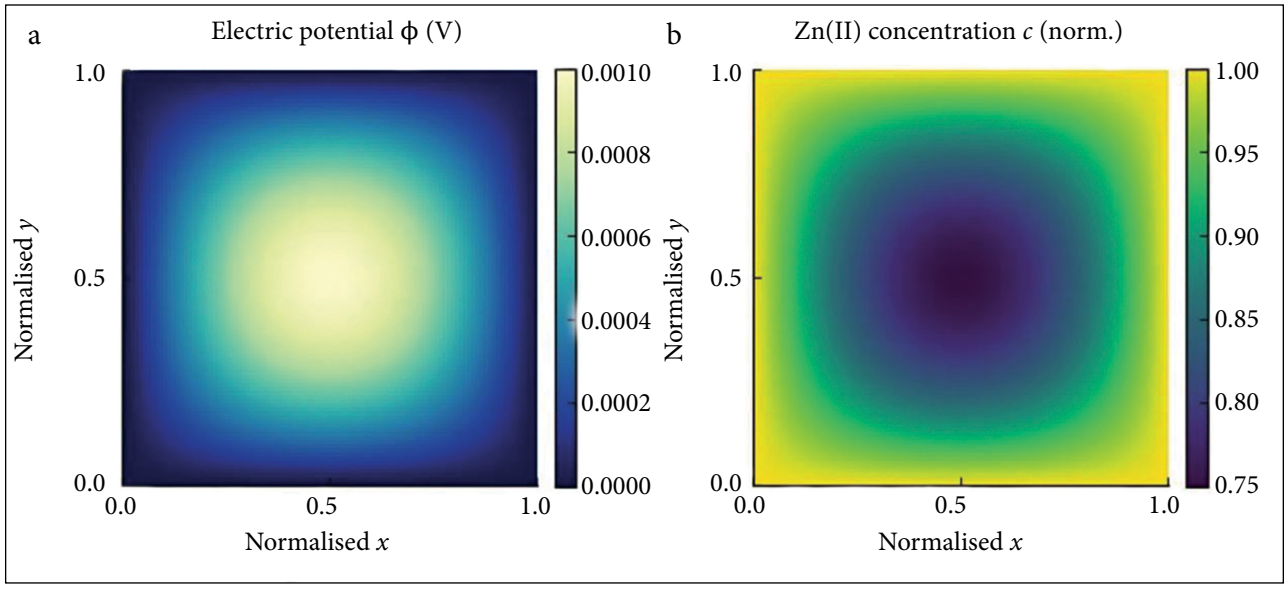

Fig. 2. PINN-predicted steady-state electric potential ϕ and Zn^{2+} concentration distributions in the beetroot leaf (both in normalised units): (a) panel shows ϕ(*x*, *y*), where a higher potential is seen in the interior (centre) of the leaf and the lower one at the edges; (b) panel shows the corresponding Zn^{2+} concentration, which is higher near the edges of the leaf and lower at the centre

no unphysical oscillations – the profile of ϕ(*x*, *y*) is smooth and symmetric, as expected given the uniform material properties and symmetric geometry assumed.

The Zn^{2+} concentration field predicted by the PINN exhibits a complementary pattern to the electric potential. As shown in Fig. 2b, the Zn^{2+} concentration *c*(*x*, *y*) is lower in the centre of the leaf and higher near the edges under steady-state conditions. In our normalised units, the model predicts about 20–25% higher Zn^{2+} concentration at the leaf periphery compared to the centre (for example, if the centre reaches a normalised 0.75 *c*, the edges are around 1 *c*). The model explains this nonuniform distribution as a consequence of the coupled diffusion and migration processes: initially, Zn^{2+} ions diffuse throughout the tissue, but as they do, the positively charged ions set up the electric potential gradient (higher in the centre) which pushes Zn^{2+} outward (since Zn^{2+} is positively charged and will move toward the lower potential). At the steady state, an equilibrium is reached where the outward electrostatic drift of Zn^{2+} (from the centre toward the edges) is balanced by inward diffusion (from the higher-concentration edges toward the lower-concentration centre). This balance results in a stable concentration gradient with Zn^{2+} accumulating near the edges of the leaf. Notably, the PINN was never told that more Zn^{2+} should be at the edges – this outcome emerged naturally from the model as it satisfied the physics of the Poisson and Nernst–Planck equations.

In addition to simulating ion distributions, we leveraged the PINN results to inform the sensor design for Zn^{2+} detection. Using the predicted Zn^{2+} concentration map ϕ(*x*, *y*), we evaluated how well different microelectrode array geometries would sample the high-concentration regions. Figure 3 compares two candidate designs: a uniform 10 × 10 grid of microelectrodes (a) versus a hexagonal close-packed array with a similar number of electrodes (b). In the uniform grid design (Fig. 3a), electrodes are spaced evenly in a Cartesian lattice. This simple layout ensures the coverage of the entire area, with each electrode roughly the same distance from its neighbours. However, one limitation of the grid is that near the edges and corners of the leaf, the spacing to the nearest electrode can be larger (since the grid extends only to the boundary and not beyond). Suppose that most Zn^{2+} accumulates at the extreme edges, as the model predicts. In that case, those regions might be undersampled by the grid (for example, the very corner of the leaf is only adjacent to one electrode in a grid, at the corner point itself).

The hexagonal array (Fig. 3b) offers a more densely packed coverage. In a hexagonal (honeycomb) pattern, each row of electrodes is offset by

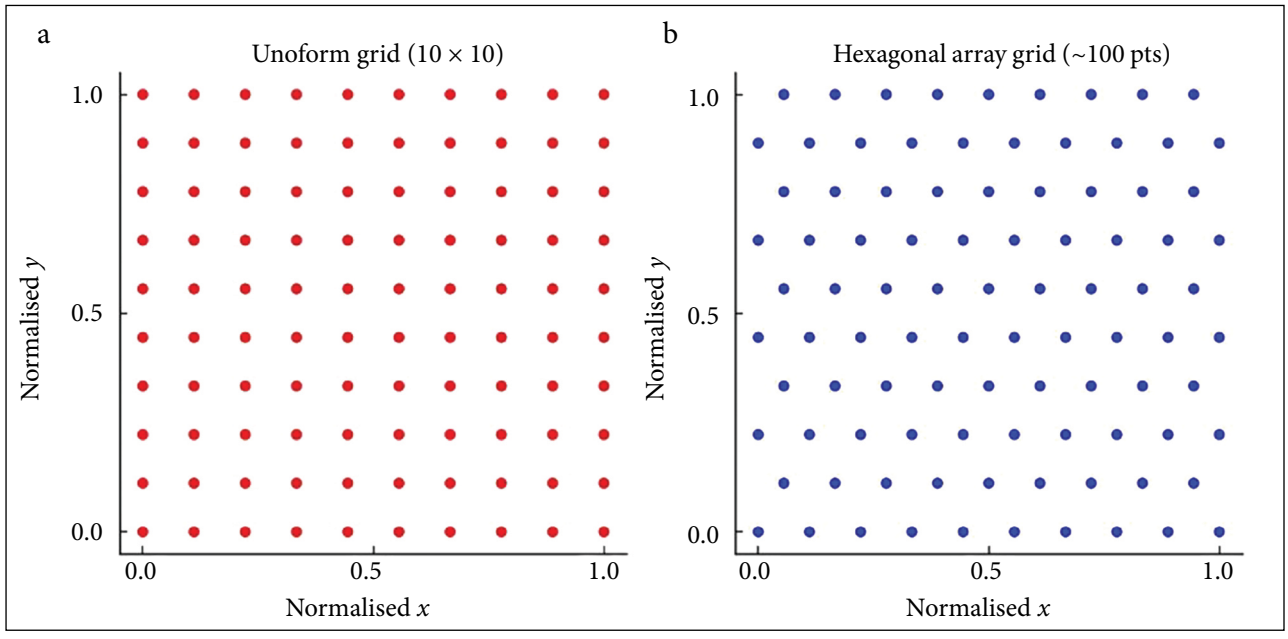

Fig. 3. Comparison of two microelectrode array designs for Zn^{2+} sensing in the leaf (top view of the sensor placement): (a) uniform grid of 10 × 10 electrodes (red points) evenly spaced across the leaf area; (b) hexagonal array of ~100 electrodes (blue points) with each row staggered (offset by half-spacing) to achieve a close-packed, honeycomb pattern. Both array layouts cover the same total area (normalised 0–1 in *x* and *y*)

half the spacing of the previous row, creating an equilateral triangular tiling. In our hexagonal design, the electrodes on one row fall in the gaps of the previous row, resulting in smaller maximum gaps between electrodes. Importantly, the proposed rows allow electrodes to be placed closer to the edges of the domain.

To determine which design is better for capturing the Zn^{2+} distribution, we considered the model's concentration field. Since the Zn^{2+} 'hotspots' are toward the leaf edges, it is crucial to have electrodes near the perimeter to detect those higher concentrations. The uniform grid does include edge electrodes (at the outermost rows/columns), but the spacing means that the very corner of the leaf is somewhat farther from the nearest electrode. In contrast, the hexagonal pattern places electrodes effectively closer to every edge point (due to the stagger), minimising any region in the leaf that is far from an electrode. From the PINN-predicted concentration map, this suggests that the hexagonal array will sample the high-Zn edge regions more densely and uniformly than the grid. In practice, this means that a hexagonal electrode layout would be more likely to detect the peak Zn signals at the margins, improving sensitivity and reducing the risk of missing localised Zn accumulations. The uniform grid might under-sample the extreme edges where *c* is highest, potentially leading to a slight underestimation of the signal.

Overall, the PINN-informed analysis indicates that a hexagonal microelectrode array is the preferred design for this application. By arranging microelectrodes in a close-packed honeycomb pattern, one ensures that the Zn^{2+} concentration field, which the model predicts to be edge-enhanced, is monitored with minimal gaps in coverage. This example illustrates how a physics-based AI model can directly guide engineering design: the knowledge gained from the PINN about where ions accumulate was used to optimise the sensor layout for a more effective detection of the target analyte.

CONCLUSIONS

In the case study, the PINN embedding Poisson's law and the Nernst–Planck equation recovered physically consistent potential and Zn^{2+} concentration fields in beetroot leaves from limited data and reproduced the observed edge accumulation of Zn, providing a mechanistic explanation. By enforcing physics, the approach reduced data requirements while improving interpretability, allowing to separate diffusion and migration contributions.

Crucially, the learned fields translated into design guidance: a hexagonal microelectrode layout is predicted to outperform a uniform grid for detecting Zn^{2+} hotspots. Overall, the results illustrate how PINNs can convert sparse measurements into actionable engineering decisions in electrochemical systems.

More broadly, the success of this PINN model in an electrochemical context shows the promise of intersecting AI techniques with physical laws. Electrochemical systems are governed by well-established principles (charge conservation, diffusion and reaction kinetics), yet they are often too complex for closed-form analytical solutions.

PINNs and related physics-informed approaches represent a promising new paradigm for accelerating innovation in electrochemistry. They empower researchers to build 'digital twins' of electrochemical systems that obey known physics, allowing a rapid virtual experimentation and optimisation. The case study on Zn^{2+} sensing in leaves is just one illustration – the same methodology can be extended to many other applications. By embracing these AI techniques that fuse data with theory, we can greatly reduce reliance on trial-and-error and empiricism, achieving more accurate models of complex phenomena and ultimately designing better electrochemical technologies. The fusion of AI with physics opens a new era in which electrochemical innovation is driven by data and theory in tandem, each informing and strengthening the other. The work presented here provides a concrete example of this intersection and its benefits. Moving forward, continued collaboration between electrochemists and AI experts will be crucial to fully realise the potential of physics-informed AI in advancing both the fundamental science and the practical applications in the electrochemical domain.

In conclusion, while the developed PINN successfully predicts the Zn^{2+} distribution patterns, several limitations should be acknowledged. First, the model assumes steady-state conditions, uniform tissue properties, and simplified leaf geometry, which may overlook microscale heterogeneities such as vascular structures or anisotropic diffusion. Second, the reaction term and boundary conditions were idealised, potentially limiting applicability to dynamic or heterogeneous environments. Third, the absence of experimental validation with soluble Zn^{2+} compounds – due to the inability of leaves to digest ZnO nanoparticles – means that the model's predictions remain unverified in real biological uptake scenarios.

ACKNOWLEDGEMENTS

The authors gratefully acknowledge Prof. Dr. Richard G. Compton (Department of Chemistry, Physical and Theoretical Chemistry Laboratory, University of Oxford, Oxford OX1 3QZ, Great Britain) and Dr. Haotian Chen (Michigan Institute for Data and AI in Society, University of Michigan, Ann Arbor, Michigan 48109-1042, United States) for their valuable guidance and insightful discussions on the modelling approach. The authors also thank Dr. Rūta Sutulienė (Institute of Horticulture and Gardening, LAMMC, Kaunas, Lithuania) for providing Swiss chard plants. This research was financed by RTO Lithuania, Project No. JV-2500-178-2023. The paper is dedicated to Prof. Valdemaras Razumas's jubilee.

Received 20 August 2025
Accepted 30 August 2025

References

1. R. K. A. Amali, H. N. Lim, I. Ibrahim, N. M. Huang, Z. Zainal, S. A. A. Ahmad, *Trends Environ. Anal. Chem.*, **31**, e00135 (2021).
2. G. F. Giordano, L. F. Ferreira, Í. R. S. Bezerra, et al., *Anal. Bioanal. Chem.*, **415**, 3683 (2023).
3. A. Mistry, A. A. Franco, S. J. Cooper, S. A. Roberts, V. Viswanathan, *ACS Energy Lett.*, **6**, 1422 (2021).
4. X. Jiang, Y. Yan, Y. Su, *Npj Mater. Degrad.*, **6**, 92 (2022).
5. H. Chen, E. Kätelhön, R. G. Compton, *J. Phys. Chem. Lett.*, **13**, 536 (2022).
6. H. Chen, M. Yang, B. Smetana, V. Novák, V. Matějka, R. G. Compton, *Angew. Chem. Int. Ed.*, **63**, e202315937 (2024).
7. M. Borah, Q. Wang, S. Moura, D. U. Sauer, W. Li, *Commun. Eng.*, **3**, 134 (2024).
8. Y. Xiong, D. Zhang, X. Ruan, et al., *Energy Storage Mater.*, **73**, 103860 (2024).
9. S. Manna, P. Paul, S. S. Manna, S. Das, B. Pathak, *Chem. Mater.*, **37**, 1759 (2025).
10. L. Jiang, C. Hu, S. Ji, H. Zhao, J. Chen, G. He, *Appl. Energy*, **377**, 124604 (2025).
11. A. P. Dmitrieva, A. S. Fomkina, C. T. Tracey, et al., *J. Mater. Chem. A*, **12**, 31074 (2024).
12. H. Wu, M. Chen, H. Cheng, T. Yang, M. Zeng, M. Yang, *J. Mater. Inform.*, **5**, 1 (2025).

13. A. Moses, D. Chen, P. Wan, S. Wang, *Mater. Today Commun.*, **37**, 107285 (2023).
14. C. Allen, S. Aryal, T. Do, et al., *Front. Microbiol.*, **13**, 1059123 (2022).
15. R. Cancelliere, M. Molinara, A. Licheri, A. Maffucci, L. Micheli, *Digit. Discov.*, **4**, 338 (2025).
16. P. Puthongkham, S. Wirojsaengthong, A. Suea-Ngam, *The Analyst*, **146**, 6351 (2021).
17. A. E. Tayfour Ahmed, Th. S. Dhahi, T. A. Attia, et al., *Heliyon*, **11**, e41338 (2025).
18. S. Husted, F. Minutello, A. Pinna, S. Le Tougaard, P. Møs, P. M. Kopittke, *Tr. Plant Sci.*, **28**, 90 (2023).
19. N. Amist, S. Khare, Niharika, Z. Azim, N. B. Singh, in: D. K. Tripathi, V. P. Singh, S. Pandey, S. Sharma, D. K. Chauhan (eds.), *Zinc in Plants: Current Knowledge and Recent Advances*, 41, Elsevier Inc. (2024).
20. M. Vaculík, T. Mišljenović, Z. Lukačová, K. Jakovljević, D. Podar, J. Kováč, in: D. K. Tripathi, V. P. Singh, S. Pandey, S. Sharma, D. K. Chauhan (eds.), *Zinc in Plants: Current Knowledge and Recent Advances*, 1, Elsevier Inc. (2024).
21. M. R. Broadley, P. J. White, J. P. Hammond, I. Zelko, A. Lux, *New Phytol.*, **173**, 677 (2007).
22. B. Sadeghzadeh, Z. Rengel, in: M. J. Hawkesford, P. Barraclough (eds.), *The Molecular and Physiological Basis of Nutrient Use Efficiency in Crops*, 1st edn., Wiley, 335 (2011).
23. J. Wang, *Biosens. Bioelectron.*, **21**, 1887 (2006).
24. W. E. Schiesser, *Spline Collocation Methods for Partial Differential Equations: With Applications in R*, 1st edn., Wiley (2017).
25. M. Abdelkader, *PINNs_rootleaves*, Python Code, Vilnius (2025) [https://github.com/Mohamed-Abdelkader94/PINNs_rootleaves].
26. L. Taiz, I. M. Møller, A. Murphy, E. Zeiger (eds.), *Plant Physiology and Development*, 7th edn., Oxford University Press, New York (2023).
27. J. Newman, K. E. Thomas-Alyea, *Electrochemical Systems*, 3rd edn., Wiley-Interscience, Hoboken (2004).

Mohamed Abdelkader, Simona Tučkutė, Rasa Pauliukaitė

FIZIKOS PAGRĮSTŲ NEURONINIŲ TINKLŲ (PINN) NAUDOJIMAS ZN^{2+} NANODALELIŲ DIFUZIJOS KARTOGRAFAVIMUI MANGOLDUOSE KARTOGRAFUOTI: SUPAPRASTINTAS DIRBTINIO INTELEKTO MODELIAVIMO METODAS